Flow and Heat Transfer in Biological Tissues: Application of Porous Media Theory

Khalil Khanafer, Abdalla AlAmiri, Ioan Pop, and Joseph L. Bull

Abstract The transport phenomena in porous media have generated increasing interest over the past several decades owing to the importance of porous media in diverse fields such as biotechnology, living structures, chemical and environmental engineering, etc. Particularly, significant advances have been achieved in applying porous media theory in modeling biomedical applications. Examples include computational biology, tissue replacement production, drug delivery, advanced medical imaging, porous scaffolds for tissue engineering and effective tissue replacement to alleviate organ shortages, and transport in biological tissues. Another important application of porous media includes diffusion process in the extracellular space (ECS) which is crucial for investigating central nervous system physiology. In this chapter, three applications namely brain aneurysm, flow and heat transfer in biological tissues, and porous scaffolds for tissue engineering are analyzed as related to the advances in porous media theory in biological applications.

1 Brain Aneurysm

1.1 Introduction

A cerebral or brain aneurysm, which is a cerebrovascular disorder, is a balloon-like bulging outward of the wall of an artery in the brain. A common location of cerebral

Khalil Khanafer
University of Michigan, Ann Arbor, MI, USA
e-mail: khanafer@umich.edu

Abdalla AlAmiri
United Arab Emirates University, Al-Ain, UAE
e-mail: alamiri@uaeu.ac.al

Ioan Pop
University of Cluj, Cluj, Romania
e-mail: pop-ioan@yahoo.co.uk; popi@math.ubbcluj.ro

Joseph L. Bull
University of Michigan, Ann Arbor, MI, USA
e-mail: khanafer@umich.edu

P. Vadász (ed.), *Emerging Topics in Heat and Mass Transfer in Porous Media*,

aneurysms is on the arteries at the base of the brain, known as the Circle of Willis (Hademenos, 1995). The bursting of an aneurysm in a brain artery or blood vessel causes bleeding into the brain or the space closely surrounding the brain called subarachnoid, which leads to a hemorrhagic stroke, brain damage and death. Recently, embolization using coils has been used widely to treat intracranial aneurysms. This endovascular coiling technique (or coil embolization), which involves the deployment of tiny platinum coils into the aneurysm through the catheter, is successfully used in the treatment of brain aneurysms by blocking blood flow into the aneurysm sac and consequently preventing rupture. Coil embolization has been found to have several advantages compared to surgical clipping. It produces significantly better patient results than surgery in terms of survival, free of disability, and a lower risk of death than in surgically-treated patients.

However, coil embolization cannot be used in cases of wide-necked irregular shaped aneurysm due to the difficulties associated with achieving complete filling of the aneurysm sac as well as the risk of coil protrusion into the parent artery (Knuckey et al., 1992). Therefore, intravascular stents have been used across the aneurysm in conjunction with coil embolization to successfully treat surgically challenging aneurysms and to improve the density of coil packing. As such, several advantages of using stents in conjunction with coils were reported in the literature. The placement of an endovascular stent may promote intra-aneurysm stasis and thrombosis (Wakhloo et al., 1994a, 1995, 1998). Further, the stent acts as a rigid endoluminal scaffold that prevents coil protrusion into the parent artery lumen (Wakhloo et al., 1998, Turjman et al., 1994) a problem frequently encountered in wide-necked aneurysms. Thus, the combination stent–coil technique allows for the dense packing of complex large, wide-necked aneurysms that are difficult to treat surgically Fig. 1.

1.2 Clinical and Experimental Studies Associated with the Treatment of Aneurysms Using Stent Implantation and Coil Placement

Experimental studies have been performed to analyze blood flow characteristics of an aneurysm after endovascular treatment using coils and stents (Szikora et al., 1994, Wakhloo et al., 1998, Turjman et al., 1994). Lieber et al. (2002) performed

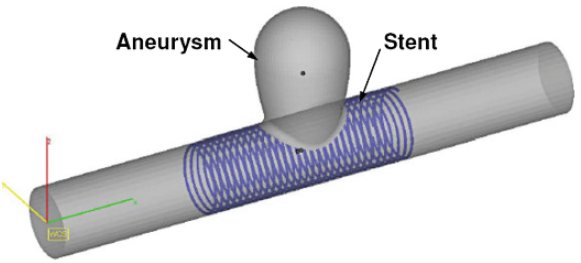

Fig. 1 Schematic diagram of the stent placed across the aneurysm neck

particle image velocimetry (PIV) measurements to study experimentally the influence of the stent filament size and stent porosity on the intra-aneurysmal flow dynamics in a sidewall aneurysm model. Their results showed that stenting significantly reduces both the intra-aneurysmal vorticity and the mean circulation inside the aneurysm. Liou et al. (2004) conducted an experimental study to investigate pulsatile flow fields in a cerebrovascular side-wall aneurysm model using helix and mesh stents. Their results showed that the hemodynamic features inside the aneurysm changed substantially with the shape of the stent. Further, comparison of the results between helix stent and mesh stent revealed that helix mesh is more favorable for endovascular treatment. The influence of aneurysm geometry and stent porosity on velocity and wall shear stress changes inside the aneurysm sac caused by stenting under physiological flow was analyzed experimentally by Rhee et al. (2002). Their results demonstrated that the intra-aneurysmal flow motion and the magnitude and pulsatility of the wall shear rate were significantly reduced in the stented aneurysm models. Canton et al. (2005) conducted an in vitro study to quantify the effect of the stents by measuring the changes in the hemodynamic forces acting on a bifurcating aneurysm model (basilar tip configuration) after the placement of flexible Neuroform stents. A digital particle image velocimetry (DPIV) system was used to measure the pulsatile velocity and shear stress fields within the aneurysm. Their results showed that peak velocity and strength of vortices inside the aneurysm sac were reduced after placing the stents. Gobin et al. (1994) observed reduction of inflow and flow stagnation at the dome with coil insertion in their in vitro model study.

Clinical experiences with stent placement and coil for cerebral aneurysm have also been reported in the literature (See for instance: Marks et al., 1994, Wakhloo et al., 1994b). Lanzino et al. (1998) reported that stent placement within the parent artery across the aneurysm reduced intra-aneurysm flow velocity which led to intra-aneurysm stasis and thrombosis and consequently preventing rupture. Kwon et al. (2006) used a new endovascular technique for treatment of cerebral aneurysms. Eight patients with wide necked aneurysms were successfully treated without complications with detachable coils using the multiple microcatheter technique as shown in Fig. 2.

1.3 Computational Studies Associated with Combined Use of Stents and Coils for the Treatment of Cerebral Aneurysms

Better understanding of the behavior of the blood flow and hemodynamics changes in various organs is a very challenging aspect in medical research. Therefore, computational fluid dynamics is considered an essential tool in the assessment and treatment of cerebral aneurysms using stents and coils. For example, Aenis et al. (1997) used finite element method, pulsatile, Newtonian flows to study the effect of stent placement on a rigid side wall aneurysm. Their results illustrated a diminished flow activity and pressure inside the stented aneurysm. Stuhne and Steinman (2004) conducted a numerical study to analyze the wall shear stress distribution and flow streamlines near the throat of a stented basilar side-wall aneurysm. The numerical simulations

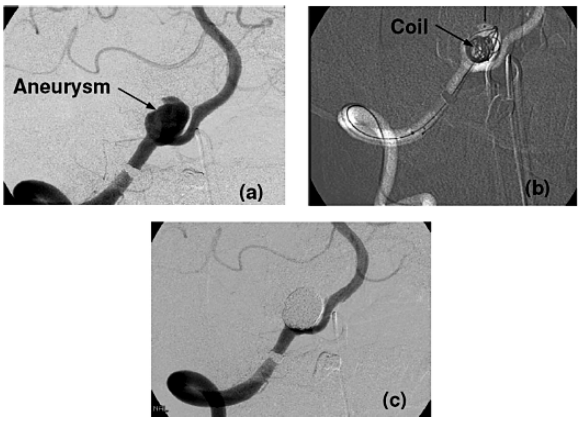

Fig. 2 (**a**) Aneurysmal Configuration visualized in 3D image, (**b**) Coil deployed to aneurismal sac and (**c**) Final angiogram shows complete occlusion of the aneurysm. A total of 333 cm platinum coil was inserted. (Reprinted from Kwon et al. (2006), with permission from Acta Neurochirurgica)

were performed assuming constant pressure at the outflow boundary of the model and specifying either steady or pulsatile flow at the inlet. For pulsatile simulations, wall shear stress (WSS) intensification was most prominent on the sides of the stent wires facing the impinging flow, while WSS reduction was most prominent on the patches of vessel lumen near wire–wire intersections. Ohta et al. (2005) analyzed hemodynamic changes in intracranial aneurysms after stent placement using a finite element modeling approach. Their work illustrated areas with stagnant flow and low shear rates.

Computational modeling of coil embolization technique in the treatment of brain aneurysms has received less attention in the literature due to the irregularly-shaped geometry of the coil. Three-dimensional pulsatile flow simulation before and after endovascular coil embolization of a terminal cerebral aneurysm was investigated by Groden et al. (2001) using in vivo data obtained by computer tomographic angiography. The filling of the aneurysm neck with platinum coils was simulated by a distribution of blocked cells. In essence, the fluid was not allowed to enter these cells. Their results showed that a complete cessation of the inflow through the aneurysm neck was achieved with a 20% filling. It should be pointed out, however, their model represents an approximate approach to determine the effect of filling the aneurysm sac with a coil. Thus, an innovative method for accurately modeling the influence of embedded coils on the flow and pressure conditions in parent vessels and the aneurysm lumen was adopted in this work utilizing a porous substrate approach. The coil embolization was modeled as a porous substrate with direction-dependent permeabilities similar to the study reported by Srinivasan et al. (1994). Srinivasan et al. (1994) developed a model for predicting the friction and heat transfer in spirally fluted tubes using porous media theory. The flute region was modeled as a porous substrate. Recently, Khanafer et al. (2006) developed a mathematical model for determining the flow field under physiological condition within a brain aneurysm filled with

coils using volume-averaged porous media approach. Their results showed that the presence of the coil significantly reduced the velocity and vorticity within the aneurysm sac.

1.4 Mathematical Formulation

The conservation equations for the coil region shown in Fig. 3 are based on the generalized flow model in porous media, which includes the effects of inertia as well as friction caused by the macroscopic shear. The generalized model, which was obtained through local volume averaging and matched asymptotic expansions, is also knows as the Brinkman-Forchheimer-Darcy model and described in rigorous detail by Vafai and Tien (1980, 1981), Nakayama (1995), Vafai and Amiri (1998) and Nield and Bejan (2006). These equations can be summarized as follows:
Continuity equation:

$$\nabla \cdot < \mathbf{v} >= 0 \tag{1}$$

Momentum equation:

$$\frac{\rho_f}{\varepsilon}\left[\frac{\partial < \mathbf{v} >}{\partial t} + < (\mathbf{v}\cdot\nabla)\mathbf{v} >\right] = -\nabla < P >^f + \frac{\mu_f}{\varepsilon}\nabla^2 < \mathbf{v} > \quad - \frac{\mu_f}{K} < \mathbf{v} > \\ - \frac{\rho_f F \varepsilon}{\sqrt{K}}[< \mathbf{v} > . < \mathbf{v} >]J \tag{2}$$

In the above equations ε is the porosity, F is the geometric function, K is the permeability, μ_f is the fluid dynamic viscosity, $\mathbf{J} = \frac{\mathbf{v}_p}{|\mathbf{v}_p|}$ is the unit vector along the pore velocity vector $\mathbf{v}_p$, $< \mathbf{v} >$ is the average velocity vector, and $< P >^f$ is the average readoff pressure. The medium permeability K can be properly modeled (Vafai, 1984, 1986, AlAmiri 2000, 2002, Khanafer et al., 2003a, b).

The porosity of the coil can be used as an index to determine the required density of coil compaction for a patient and consequently reduces the occurrence of rupture during the deployment of the coil. The porosity of the coil depends strongly on the

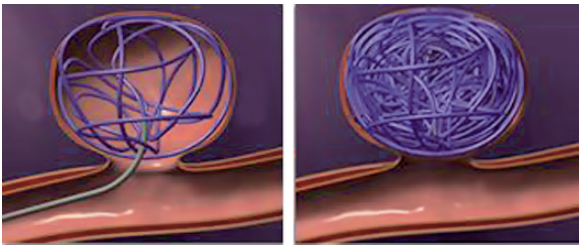

Fig. 3 A schematic diagram of an aneurysm filled with coil (Reprinted with permission from the American Society of Interventional and Therapeutic Neuroradiology)

volume of the aneurismal sac. More experimental studies are necessary to correlate the porosity of the coil to the density of the coil and the volume of the aneurysm sac. An analytical expression of the porosity ε can be easily derived for a helix stent, which is a spring-like in shape for better control of porosity (Fig. 1), as follows.

$$\varepsilon = \frac{L - n \times d}{L} \tag{3}$$

Where L is the length of the stent, n is the number of stent loops (or filaments), and d is the diameter of the wire. The effect of the stent on the inflow into the aneurysm can be characterized by the blocking ratio defined as:

$$C = \frac{n \times d}{L} = 1 - \varepsilon \tag{4}$$

2 Flow and Heat Transfer in Biological Tissues

2.1 Introduction

The development of mathematical models for flow and heat transfer in living tissues has been a topic of interest for various physicians and engineers. The accurate description of the thermal interaction between vasculature and tissues is essential for the advancement of medical technology in treating fetal diseases such as tumor. Currently, mathematical models have been used extensively in the analysis of hyperthermia in treating tumors, cryosurgery, and many other applications. Hyperthermia treatment has been demonstrated effective as cancer therapy in recent years. Its objective is to raise the temperature of pathological tissues above cytotoxic temperatures (41–45 °C) without overexposing healthy tissues (Overgaard et al., 1996, Oleson et al., 1984, Dewhirst and Samulski, 1988, Field and Hand, 1990). The success of hyperthermia treatment strongly depends on the knowledge of the heat transfer processes in blood perfused tissues. As such, accurate thermal modeling is essential for effective treatment by hyperthermia. Khanafer et al. (2007) conducted a numerical study to determine the influence of pulsatile laminar flow and heating protocol on temperature distribution in a single blood vessel and tumor tissue receiving hyperthermia treatment using physiological velocity waveforms. Their results showed that the presence of large vessels has a significant effect on temperature distributions and must be accounted for when planning hyperthermia treatment (Fig. 4). Further, uniform heating scheme was found to exhibit larger temperature distribution than for pulsed heating scheme which may induce areas of overheating (beyond the therapeutic regions) that could damage normal tissues (Fig. 5).

Heat transport in biological tissues, which is usually expressed by the Bioheat Equation, is a complicated process since it involves thermal conduction in tissues, convection and perfusion of blood, and metabolic heat generation. Therefore, several authors have developed mathematical models of bioheat transfer

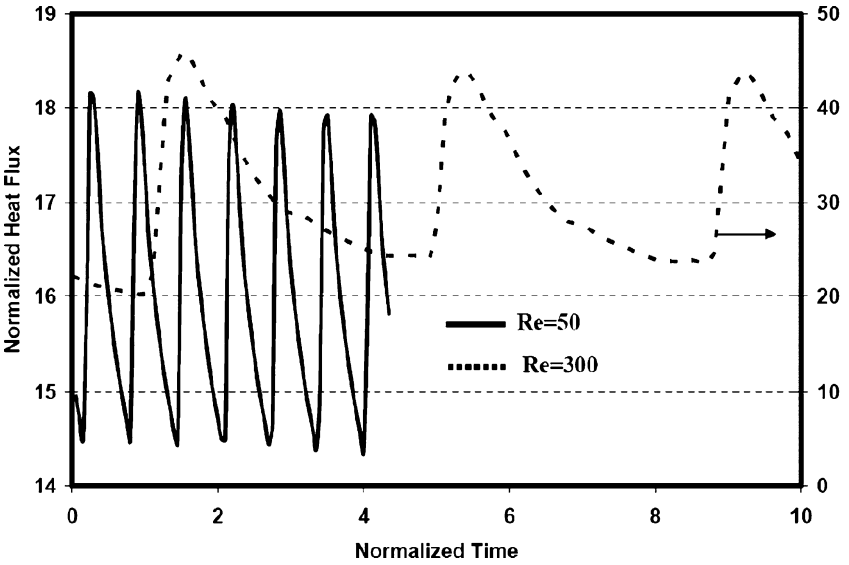

Fig. 4 Temporal variation of the normalized heat flux for different Reynolds numbers

as an extended/modified version of the original work of Pennes (1948) as reported by Charny (1992) and Arkin et al. (1994). Below is a comprehensive summary of different thermal models and their limitations for blood perfused tissues.

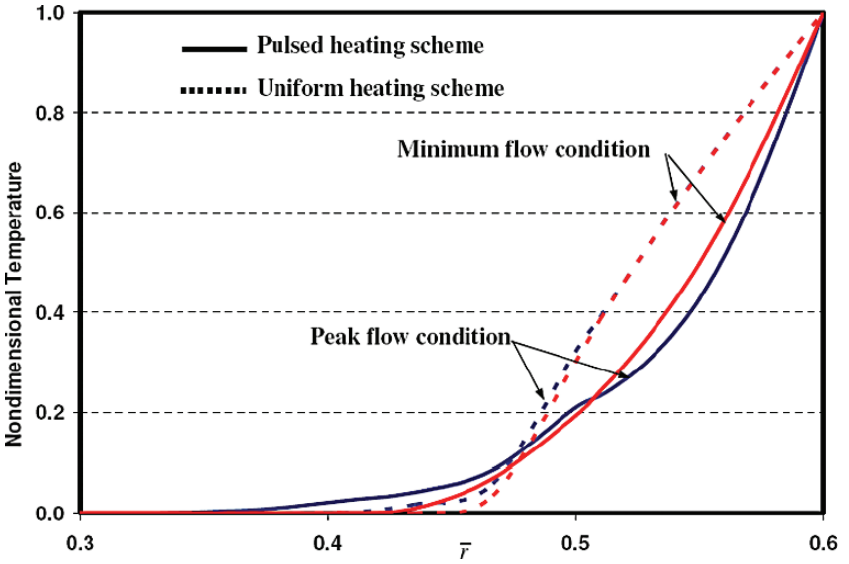

Fig. 5 Influence of the heating protocol on the temperature distribution at various flow conditions (Re = 300)

2.2 Thermal Models for Blood Perfused Tissues

2.2.1 The Pennes Bioheat Equation

The Pennes (1948) model was originally designed for predicting heat transfer in human forearm. Pennes modeled the net heat transfer (q_p) from the blood to the tissue to be proportional to the temperature difference between the arterial blood entering the tissue and the venous blood leaving the tissue as follows:

$$q_p = \omega \rho_b c_b (T_b - T) \tag{5}$$

where ω is the blood volumetric perfusion rate, ρ_b is the blood density, and c_b is the blood specific heat. Because the perfusion rate (ω) could not be directly measured, Pennes varied this parameter to fit his experimental data. Also, Pennes derivation assumed that the arterial blood temperature T_b is uniform throughout the tissue while he considered the venous temperature to be equal to the tissue temperature which is denoted by T at the same point. The equation that Pennes developed is expressed in its simplest form as:

$$\rho\, c_p \frac{\partial T}{\partial t} = \nabla \cdot (k \nabla T)) + \omega \rho_b c_b (T_b - T) + q_m \tag{6}$$

where ρ, c_p, k, and q_m are tissue density, tissue specific heat, tissue thermal conductivity, and uniform rate of metabolic heat generation in the tissue layer per unit volume, respectively. Due to the inherent simplicity of Pennes bio-heat transfer model (assume uniform thermal conductivity, perfusion rate, and metabolic heating) Pennes model was implemented in various biological research works such as therapeutic hyperthermia for the treatment of cancer (See for instance: Roemer and Cetas, 1984, Charny and Levin, 1988, 1989).

2.2.2 Wulff Continuum Model

Several investigators have questioned the validity of the fundamental assumptions of Pennes bio-heat equation. Wulff (1974) was one of the first studies that directly criticized the assumptions of Pennes model. Since blood may convect heat in any direction, Wulff (1974) assumed that the heat transfer between flowing blood and tissue should be modeled to be proportional to the temperature difference between these two media rather than between the two blood stream temperatures (temperature of the blood entering and leaving the tissue). Thus, the energy flux at any point in the tissue is expressed by:

$$q = -k \nabla T + \rho_b h_b \mathrm{v}_h \tag{7}$$

where v_h is the local mean blood velocity, and T is the tissue temperature. The specific enthalpy of the blood h_b is given by:

$$h_b = \int_{T_o}^{T_b} c_p(T_b^*)dT_b^* + \frac{P}{\rho_b} + \Delta H_f(1-\phi) \tag{8}$$

Where P is the system pressure, ΔH_f is the specific enthalpy of the metabolic reaction, and ϕ is the extent of reaction, respectively. Thus, the energy balance equation can be written as

$$\rho\, c_p \frac{\partial T}{\partial t} = -\nabla \bullet q = -\nabla \bullet (-k\nabla T + \rho_b h_b \mathrm{v}_h) = \nabla \bullet \left[k\nabla T - \rho_b \mathrm{v}_h \int_{T_o}^{T_b} c_p(T_b^*)dT_b^* + \frac{P}{\rho_b} + \Delta H_f(1-\phi) \right] \tag{9}$$

The above equation can be simplified by neglecting the mechanical work term (P/ρ_b), setting the divergence of the product $(\rho_b \mathrm{v}_h)$ to zero, and assuming constant physical properties as follows:

$$\rho\, c_p \frac{\partial T}{\partial t} = k\nabla^2 T - \rho_b \mathrm{v}_h \left(c_p \nabla T_b - \Delta H_f \nabla \phi \right) \tag{10}$$

Wulff (1974) assumed that T_b is equivalent to the tissue temperature T because blood in the microcirculation is in thermal equilibrium with the surrounding tissue. Therefore, the final form of bio-heat equation that was derived by Wulff (1974) is:

$$\rho\, c_p \frac{\partial T}{\partial t} = k\nabla^2 T - \rho_b \mathrm{v}_h c_p \nabla T + q_m \tag{11}$$

2.2.3 Klinger Continuum Model

Since the effects of non-unidirectional blood flow were neglected in Pennes model, Klinger (1974) emphasized that the convection heat transfer caused by the blood flow inside the tissue should be modeled to take into an account the spatial and temporal variation of the velocity field and heat source. Thus, the general heat transport equation can be written as:

$$\rho\, c \frac{\partial T}{\partial t} + (\rho\, c)\, \mathbf{v}\, \nabla T = k\nabla^2 T + q \tag{12}$$

This model assumed constant physical properties of tissue and incompressible blood flow.

2.2.4 Continuum Model of Chen and Holmes (CH)

In the Chen and Holmes (CH) model (1980), the control volume occupied by the tissue and blood vessels was divided into two separate volumes: one for solid tissue

and the other consisted only of blood in the vascular space within the blood vessels. Using volume-averaged technique, the energy balance equations for both the solid tissue space and vascular spaces can be written as:

Solid Phase:

$$dV_s(\rho\, c)_s \frac{\partial T_s}{\partial\, t} = dQ_{ks} + dQ_{bs} + dQ_m \tag{13}$$

Fluid Phase:

$$dV_b(\rho\, c)_b \frac{\partial T_b}{\partial\, t} = dQ_{kb} - dQ_{bs} + \int_S (\rho\, c)_b T\mathbf{v}d\mathbf{s} \tag{14}$$

Where dV_s is the differential volume of the solid phase, dV_b is the differential volume of the blood in the vascular space, dQ_{ks} is the energy transferred by conduction, dQ_{bs} is the energy transferred gain in the control volume from the blood space, dQ_m is the metabolic heating energy, dQ_{kb} is the energy gain in the vascular space by conduction, and the integral term in Eq. (14) denotes the energy transfer by convection as the blood flows across the surface area S at velocity $\mathbf{v}$. Therefore, the energy balance for the tissue space is derived by the addition of Eqs. (13–14) and division of the result by the total control volume dV yields the following:

$$(\rho\, c)\frac{\partial T_t}{\partial t} = q_k + q_m + q_p \tag{15}$$

Where q_k is the heat transfer by conduction per unit volume, q_m is the metabolic heat per unit volume, and q_p is the perfusion energy per unit volume. Here ρ, c and T_t denote the local mean density, specific heat, and temperature of the tissue based on the volume average as follows:

$$T_t = \frac{1}{\rho\, c}\left[\left(1 - \frac{dV_b}{dV}\right)(\rho\, c)_s T_s + \frac{dV_b}{dV}(\rho\, c)_b T_b\right] \tag{16}$$

$$\rho = \left(1 - \frac{dV_b}{dV}\right)\rho_s + \frac{dV_b}{dV}\rho_b \;\&\; c = \frac{1}{\rho}\left[\left(1 - \frac{dV_b}{dV}\right)(\rho\, c)_s + \frac{dV_b}{dV}(\rho\, c)_b\right] \tag{17}$$

The total heat transfer by conduction per unit volume (q_k) in the tissue control volume is expressed by:

$$q_k = \frac{Q_{ks} + Q_{kb}}{dV} = \nabla \bullet \left(k_{eff}\nabla T_t\right) \tag{18}$$

where k_{eff} is the effective thermal conductivity of the combined tissue and vascular spaces. The effective thermal conductivity is written as:

$$k_{eff} = \varepsilon\, k_b + (1-\varepsilon) k_s \tag{19}$$

Since $\varepsilon = \frac{dV_b}{dV} \sim \frac{dV_b}{dV_s} << 1$ it follows that $k_{eff} \cong k_s$. Therefore, the effective thermal conductivity is equal to the thermal conductivity of the solid tissue medium, k_s.

Chen and Holmes (1980) expressed the perfusion term (or the bulk flow term) q_p as follows:

$$q_p = q_{p(1)} + q_{p(2)} + q_{p(3)} = (\rho\, c)_b \omega^* \left(T_a^* - T_s\right) - (\rho\, c)_b \mathbf{v}_p \bullet \nabla T_s - \nabla \bullet k_p \nabla T_s \tag{20}$$

where $q_{p(1)}$ represents the effect of blood flow on tissue temperature around large vessels, T_s is the temperature of the solid tissue component of the tissue-blood model, ω^* is the total perfusion associated with the blood flow to the tissue only from the vessels, and T_a^* is the temperature of the blood within the largest vessels. $q_{p(2)}$ corresponds to the heat transfer that takes place as a result of the flowing blood, and $\rho_b \mathbf{v}_b$ is the mass flux of the blood through the tissue. Because of the thermal equilibrium, the blood temperature is equal to the solid tissue temperature everywhere in the control volume. $q_{p(3)}$ characterizes the heat transfer due to the small temperature changes and is proportional to the tissue temperature gradient. k_p is the perfusion thermal conductivity. Therefore, the new bio-heat equation for Chen and Holmes (1980) is written as

$$\rho\, c \frac{\partial T_t}{\partial t} = \nabla \bullet k_{eff} \nabla T_t + (\rho\, c)_b \omega^* \left(T_a^* - T_t\right) - (\rho\, c)_b \mathbf{v}_p \bullet \nabla T_t + \nabla \bullet k_p \nabla T_t + q_m \tag{21}$$

where T_s is replaced by the volume-weighted continuum temperature (T_t). This is reasonable as long as $\varepsilon << 1$.

2.2.5 The Weinbaum, Jiji, and Lemons (WJL) Bio-Heat Equation Model

Weinbaum and colleagues (1979, 1984a, b) derived the bio-heat equation based on a hypothesis that small arteries and veins are parallel and the flow direction is countercurrent resulting in counterbalanced heating and cooling effects. Accordingly, they modified the thermal conductivity in the Pennes equation by means of an 'effective conductivity' which is a function exclusively of the blood flow rate and vascular geometry. They also showed that isotropic blood perfusion between the countercurrent vessels can have a significant influence on heat transfer in regions where the countercurrent vessels are under 70 μm diameter. Neglecting axial conduction, the artery and vein energy balances are written as:

$$(\rho\, c)_b \frac{d}{ds}\left(n\pi\, a^2 \bar{u} T_a\right) = -n q_a - (\rho\, c)_b (2\pi\, a\, n\, g) T_a \tag{22}$$

$$(\rho\, c)_b \frac{d}{ds}\left(n\pi\, a^2 \bar{u} T_{\mathrm{v}}\right) = -n q_{\mathrm{v}} - (\rho\, c)_b (2\pi\, a\, n\, g) T_{\mathrm{v}} \tag{23}$$

where q_a denotes the heat loss from the artery by conduction through its wall per unit length and q_{v} is the heat gain by conduction per unit length through the vein wall into the vein. T_a, and T_{v} are the bulk mean temperatures inside the blood vessel, and g is the perfusion bleed-off per unit vessel surface area. For an equal-size artery-vein pair, subtracting Eq. (23) from Eq. (22) yields:

$$(\rho\, c)_b \left[\frac{d}{ds}\left(n\pi\, a^2 \bar{u} T_a\right) - \frac{d}{ds}\left(n\pi\, a^2 \bar{u} T_{\mathrm{v}}\right) \right] = -n(q_a - q_{\mathrm{v}}) - (\rho\, c)_b (2\pi\, a\, n\, g)(T_a - T_{\mathrm{v}}) \tag{24}$$

where the term on the left-hand side represents the total heat exchange blood in the countercurrent vessels and the surrounding tissue. This term can be balanced by conduction and metabolic heating as follows:

$$(\rho\, c)_b \left[\frac{d}{ds}\left(n\pi\, a^2 \bar{u} T_a\right) - \frac{d}{ds}\left(n\pi\, a^2 \bar{u} T_{\mathrm{v}}\right) \right] = \nabla \bullet (k_t \nabla T_t) + q_m \tag{25}$$

The rate of the energy entering and leaving the tissue control volume can be expressed as:

$$q_a - q_{\mathrm{v}} = (\rho\, c)_b (\pi\, a^2 \bar{u}) \frac{d}{ds} \left[T_{\mathrm{v}} - T_{\mathrm{a}} \right] \tag{26}$$

where,

$$q_a = -(\rho\, c)_b (\pi\, a^2\, \bar{u}) \frac{dT_a}{ds} \;\&\; q_{\mathrm{v}} = -(\rho\, c)_b (\pi\, a^2\, \bar{u}) \frac{dT_{\mathrm{v}}}{ds} \tag{27}$$

Thus, Eq. (25) can be written in the final form as:

$$(\rho\, c)_b (n\pi\, a^2 \bar{u}) \frac{d}{ds} \left[T_a - T_{\mathrm{v}} \right] - (\rho\, c)_b (n\, 2\pi\, a\; g)(T_a - T_{\mathrm{v}}) = \nabla \bullet (k_t \nabla T_t) + q_m \tag{28}$$

2.2.6 The Weinbaum and Jiji Bio-Heat Equation Model

Weinbaum and Jiji (1985) derived a simplified, single equation model to study the effect of blood flow on the tissue temperature variations. This is because Eq. (26) cannot be solved for T_t since both T_a and T_{v} are unknowns. Therefore, the mean tissue temperature can be approximated as:

$$T_t \cong \frac{T_a + T_{\mathrm{v}}}{2} \tag{29}$$

Thus, the magnitude of the difference $(q_a - q_{\mathrm{v}})$ is much smaller than the magnitude of either q_a or q_{v}. Moreover, Weinbaum and Jiji (1985) assumed that the tissue around the vessel pair is a pure conduction region such that:

$$q_a \cong q_{\mathrm{v}} = \sigma\, k_t (T_a - T_{\mathrm{v}}) \tag{30}$$

where σ is a geometrical factor given by:

$$\sigma = \frac{\pi}{cosh^{-1}(L_s/a)} \tag{31}$$

The ratio L_s/a denotes the ratio of the vessel spacing to vessel diameter. Equations (27), (29), and (30) are solved to obtain an equation for the artery-vein temperature difference and the tissue temperature gradient:

$$T_a - T_v = -\frac{\pi\, a^2\, \bar{u}\, (\rho\, c)_b}{\sigma\, k_t} \frac{dT_t}{ds} \tag{32}$$

Substituting Eq. (32) in the original model of WJL; Eq. (24), yields a new bioheat equation proposed by Weinbaum and Jiji (1985) as follows:

$$\frac{n\pi^2\, ak_b}{4k_t} Pe \left(\frac{d}{ds} \left[\frac{a\, Pe}{\sigma} \frac{dT_t}{ds} \right] - \frac{2g\, Pe}{\sigma\, \bar{u}} \frac{dT_t}{ds} \right) = -\nabla \bullet k_t \nabla T_t - q_m \tag{33}$$

Where Pe is the Peclet number; which is defined as $Pe = \dfrac{2a(\rho\, c)_b \bar{u}}{k_b}$.

2.2.7 Other Models

Baish (1994) developed a new bioheat transfer model for a perfused tissue based on solving conjugate convection of the blood coupled to the three-dimensional conduction in the extravascular tissue while accounting for a statistical interpretation of the calculated temperature field. He illustrated that Pennes model of bioheat transfer equation accurately determines the mean tissue temperature except when the arteries and veins are in closely spaced pairs. Moreover, Baish (1994) demonstrated the dependence of the temperature distribution on the flow rate and the vascular geometry. Wissler (1987) vigorously criticized the assumptions that used in deriving Weinbaum and Jiji (1985) model. In particular, Wissler (1987) indicated that Weinbaum and Jiji (1985) assumed that the mean temperature in the neighborhood of an artery–vein pair is the arithmetic mean of the arterial and venous blood at the point of entry. Moreover, Wissler (1987) questioned the basis that the temperature gradient is proportional to the temperature difference between the artery–vein pair which was used in the derivation of Weinbaum and Jiji model.

2.3 Mathematical Modeling of Bioheat Equation Using Porous Media Theory

Transport phenomena in porous media have received continuing interest in the past five decades. This interest stems from its importance in many industrial and clinical applications (Bejan et al., 2004, Ingham and Pop, 2002, 2005, Ingham et al., 2004,

Pop and Ingham, 2001, Vafai, 2000, 2005, Khanafer et al., 2003a, b). Moreover, complicated and interesting phenomena can be modeled using porous media concept. Recently, Xuan and Roetzel (1997, 1998) employed porous media concept to model tissue-blood system composed mainly of tissue cells and interconnected voids that contain either arterial or venous blood. The thermal energy exchange between the tissue and blood was modeled using the principle of local thermal non-equilibrium as described in the works of Amiri and Vafai (1994, 1998), Alazmi and Vafai (2002), Khashan et al. (2005, 2006), and Lee and Vafai (1999). Thus, two energy equations were derived for the blood and tissue, respectively:

$$\varepsilon(\rho\, c)_b \left(\frac{\partial < T >^b}{\partial t} + < \mathbf{u} >^b \cdot \nabla < T >^b \right) = \nabla \cdot \left(\mathbf{k}_b^a \cdot \nabla < T >^b \right) + h_{bs} \left[< T >^s - < T >^b \right] \quad (34)$$

$$(1-\varepsilon)(\rho\, c)_s \frac{\partial < T >^s}{\partial t} = \nabla \cdot \left(\mathbf{k}_s^a \cdot \nabla < T >^s \right) - h_{bs} \left[< T >^s - < T >^b \right] + (1-\varepsilon) q_m \quad (35)$$

where $< T >^b$, $< T >^s$, $\mathbf{k}_b^a$, $\mathbf{k}_s^a$, $< \mathbf{u} >^b$ and h_{bs}, and ε are the local volume-averaged arterial blood temperature, local volume-averaged solid tissue temperature, blood effective thermal conductivity tensor, solid tissue effective thermal conductivity tensor, blood velocity vector, and interstitial convective heat transfer coefficient, respectively. For isotropic conduction, the effective thermal conductivity k_b^a of blood and solid tissue k_s^a can be expressed as:

$$k_b^a = \varepsilon\, k_b \text{ and } k_s^a = (1-\varepsilon) k_s \quad (36)$$

The heat exchange between the blood and the tissue is expressed as: $h_{bs} \left[< T >^s - < T >^b \right]$. Further, Xuan and Roetzel (1997, 1998) considered an effective thermal conductivity for the blood to account for blood dispersion. The concept of thermal dispersion is well established in the theory of porous media as presented in the works of Amiri and Vafai (1994, 1998). Due to insufficient knowledge about the thermal and anatomic properties of the tissue, velocity field of the blood, and interstitial convective heat transfer coefficients, the local thermal equilibrium model represents a good approximation for determining the temperature field in applications involving small size blood vessels ($\varepsilon << 1$). This implies that blood flowing in these small vessels will be completely equilibrated with the surrounding tissue. Therefore, Eqs. (34) and (35) reduce to the following equation (Khanafer and Vafai, 2001, Marafie and Vafai, 2001):

$$[(\rho\, c)_b \varepsilon + (1-\varepsilon)(\rho\, c)_s] \frac{\partial < T >}{\partial\, t} + \varepsilon(\rho\, c)_b < \mathbf{u} >^b \cdot \nabla < T > = \nabla \left[\left(\mathbf{k}_s^a + \mathbf{k}_b^a \right) \cdot \nabla < T > \right] + q_m(1-\varepsilon) \quad (37)$$

The second term on the left hand side of the above equation represents the heat transfer due to the blood perfusion. The perfusion source term in Pennes

model was derived based on a uniform blood perfusion assumption and is equal to $(\rho\, c)_b \omega (T_b - T)$. In hyperthermia applications, tissue may absorbs energy from external source such as electromagnetic or ultrasonic radiation and therefore another heat source term should be added to the right side of Eq. (37) as follows:

$$[(\rho\, c)_b \varepsilon + (1-\varepsilon)(\rho\, c)_s] \frac{\partial < T >}{\partial\, t} + \varepsilon (\rho\, c)_b < \mathbf{u} >^b \cdot \nabla < T > = \nabla \left[\left(\mathbf{k}_s^a + \mathbf{k}_b^a \right) \cdot \nabla < T > \right] + q_m (1-\varepsilon) + q_h (1-\varepsilon) \tag{38}$$

From above, one can note that the theory of porous media can be used to develop a more robust bioheat model since it allows including the effect of blood thermal dispersion, porosity variation, effective tissue conductivity, and effective tissue capacitance, and the exact heat transfer exchange between the blood and tissue. However, Pennes equation ignores all these effects. Tables 1 and 2 summarize the previously discussed bioheat transfer models in this work.

3 Tissue Engineering

3.1 Introduction

Tissue engineering is an interdisciplinary field that involves chemical and material engineering, biology, reactor engineering, and medicine to develop viable biological substitutes for the repair or regeneration of human tissue or organ function (Lavik and Langer, 2004, Lanza et al., 2000). Examples of tissue-engineered substitutes that are currently being investigated include skin, cartilage, bone, vascular, heart, breast and liver (Masood et al., 2005). A large number of Americans suffer organ and tissue loss every year from accidents, birth defects, diseases, hereditary disorders, etc. Approximately 72,000 American people were on the waiting list for an organ transplant in 2000. Only 23,000 transplant were performed (Port, 2002).

In order to achieve significant tissue structures, there must be appropriate transport of nutrients to and waste from the cells as they begin to form a tissue or organ (Lavik and Langer, (2004). Various types of bioreactors have been used to culture cells for tissue regeneration or repair such as spinner flask (Sikavitsas et al., (2002), rotating wall vessels (Carrier et al., (1999), and perfusion bioreactors (Bancroft et al., (2002). The aim of the bioreactor is to provide suitable nutrients and oxygen flow and many of the biophysical and biochemical conditions necessary to produce a functional artificial tissue. Thus, bioreactor design is critical for the development of certain tissues (Bancroft et al., 2002).

3.2 Porous Scaffolds for Tissue Engineering

The efficient design and manufacture of a complex scaffold with optimum porosity and interconnectivity is significant for tissue engineering applications. The essential principle of tissue engineering is to combine a scaffold with cells for tissue

Table 1 Summary of bioheat transfer models

Model	Mathematical model
Pennes (1948)	$\rho\, c_p \frac{\partial T}{\partial t} = \nabla \cdot (k \nabla T)) + \omega \rho_b c_b \,(T_b - T) + q_m$
Wulff (1974)	$\rho\, c_p \frac{\partial T}{\partial t} = k \nabla^2 T - \rho_b \mathrm{v}_h c_p \nabla T + q_m$
Klinger (1974)	$(\rho\, c) \frac{\partial T}{\partial t} + (\rho\, c) \mathbf{v}\, \nabla T = k \nabla^2 T + q$
CH (1980)	$\rho\, c \frac{\partial T_t}{\partial t} = \nabla \bullet k_{eff} \nabla T_t + (\rho\, c)_b \omega^* \left(T_a^* - T_t\right) - (\rho\, c)_b \mathbf{v}_p \bullet \nabla T_t - \nabla \bullet k_p \nabla T_t + q_m$
WJL (1979, 1984a, b)	$(\rho\, c)_b (n \pi\, a^2 \bar{u}) \frac{d}{ds} \left[T_a - T_{\mathrm{v}}\right] - (\rho\, c)_b (n 2\pi\, a\, g)(T_a - T_{\mathrm{v}}) = \nabla \bullet (k_t \nabla T_t) + q_m$
WJ (1985)	$\frac{n \pi^2 a k_b}{4 k_t} Pe \left(\frac{d}{ds} \left[\frac{a\, Pe}{\sigma} \frac{dT_t}{ds} \right] - \frac{2 g Pe}{\sigma \bar{u}} \frac{dT_t}{ds} \right) = -\nabla \bullet k_t \nabla T_t - q_m$
Amiri and Vafai (1994, 1998, 2002), Khanafer et al. (2003a,b) Xuan and Roetzel (1997, 1998)	$\varepsilon(\rho\, c)_b \left(\frac{\partial \langle T \rangle^b}{\partial t} + < \mathbf{u} >^b \cdot \nabla < T >^b \right) = \nabla \cdot \left(\mathbf{k}_b^a \cdot \nabla < T >^b \right) + h_{bs} \left[< T >^s - < T >^b \right]$
	$(1 - \varepsilon)(\rho\, c)_s \frac{\partial \langle T \rangle^s}{\partial t} = \nabla \cdot \left(\mathbf{k}_s^a \cdot \nabla < T >^s \right) - h_{bs} \left[< T >^s - < T >^b \right] + (1 - \varepsilon) q_m$
Vafai and co-workers (1994, 1998, 2001, 2002, 2003) Xuan and Roetzel (1997, 1998)	$[(\rho\, c)_b \varepsilon + (1 - \varepsilon)(\rho\, c)_s] \frac{\partial < T >}{\partial t} + \varepsilon (\rho\, c)_b < \mathbf{u} >^b \cdot \nabla < T > = \nabla \left[\left(\mathbf{k}_s^a + \mathbf{k}_b^a \right) \cdot \nabla < T > \right] + q_m (1 - \varepsilon)$

CH: Chen and Holmes, WJ: Weinbaum, Jiji, WJL: Weinbaum, Jiji, and Lemons

Table 2 Summary of bioheat models

Bio-heat model	Main characteristics
Pennes (1948)	• Simple model • Assumed uniform physical properties and metabolic heating • Based on uniform perfusion • Heat transfer between flowing blood and tissue was modeled to be proportional to the temperature difference between the two blood stream temperatures
Wulff (1974)	• Modified version of Pennes model • Assumed thermal equilibrium between flowing blood and surrounding tissue. • Modified perfusion term • Assumed uniform mean blood velocity
Klinger (1974)	• Assumed constant physical properties • Incompressible blood flow • Includes convection heat transfer by blood flow inside the tissue • Assume spatial and temporal variation of the velocity field and heat source
CH (1980)	• Use two separate volumes: one for solid tissue and one for blood • The total heat transfer by conduction relates to heat transfer by conduction in the solid tissue and in the vascular space • The total perfusion term corresponds to: The effect of blood flow on tissue temperature around large vessels, heat transfer that takes place as a result of the flowing blood, and heat transfer due to the small temperature changes • Used solid tissue thermal conductivity for the effective thermal conductivity since the vascular space is much smaller than the tissue volume • Introduced perfusion conductivity tensor in the bio-heat equation

Table 2 (continued)

Bio-heat model	Main characteristics
WJL (1979, 1984)	• Based on a hypothesis that small arteries and veins are parallel and the flow direction is countercurrent resulting in counterbalanced heating and cooling effects • Derived coupled energy equations for artery-vein pair and tissue • Utilizes the effective conductivity which is a function of blood flow rate and vascular geometry • Assume isotropic blood perfusion between the countercurrent vessels
WJ (1985)	• The mean tissue temperature is approximated by an average temperature of the bulk mean temperatures inside the blood vessel • Valid when arteries and veins are close leading to negligible blood perfusion effects • Assumed that the tissue around the vessel pair is a pure conduction region • Utilizes an effective conductivity as function of the perfusion rate
Wissler (1987)	• Avoids assumptions of the Weinbaum and Jiji model
Porous Media Model (Local thermal equilibrium principle) Khanafer and Vafai (2001), Khanafer et al. (2003), Amiri and Vafai (1994, 1998), Xuan and Roetzel (1997, 1998), Marafie and Vafai (2001)	This model modifies Pennes equation by accounting for the following effects: • variable tissue porosity • effective tissue conductivity • effective tissue capacitance • blood dispersion
Porous Media Model (Local thermal non-equilibrium principle) Amiri and Vafai (1994, 1998), Xuan and Roetzel (1997, 1998), Alazmi and Vafai (2002), Khanafer and Vafai (2001)	• This model requires more knowledge about the thermal and anatomic properties of the tissue, velocity field of the blood, and interstitial convective heat transfer coefficients • This model considers the following effect: – variable tissue porosity – blood dispersion – effective tissue conductivity – effective tissue capacitance

replacement or repair. The scaffold provides a temporary biomechanical profile until the cells produce their own matrix proteins and a full tissue (Masood et al., (2005). Masood et al. (2005) addressed the issue of developing an efficient methodology to design and manufacture a scaffold structure using a novel approach based on fused deposition modeling (FDM) rapid prototyping (RP) technology. They derived a theoretical expression for the porosity of one horizontal layer of a cylindrical model created on the FDM process as follows:

$$\varepsilon_{theortical} = \frac{V_{pore,layer}}{V_{part,layer}} = 1 - (1 - \varepsilon_{initial}) \left\{ RW \left[\sum_{n=0}^{n=N_r} W_n \right] N_r + (N_r - 1) RG \times \pi D / N_r \right\} / t$$

$$\varepsilon_{initial} = 1 - W_{\mathrm{mod}\,el} / \left\{ \rho_{material} \times N_L \times t \times RW \left[\sum_{n=0}^{n=N_r} W_n \right] N_r \right\} \tag{39}$$

where D is the diameter, H is the height of the cylindrical model, W_{model} is the average weight of the model when an RG setting is taken as zero, RG is the raster gap, RW is road width, t is the layer thickness, $\rho_{material}$ is the density of the material, W_n is the width of nth road from the center of the cylindrical layer, N_r and N_L are the number of raster lines and the number of layers, respectively, defined as follows:

$$N_r = (D + RG)/(RW + RG) \;\&\; N_L = H/t \tag{40}$$

Porter et al. (2005) used the Lattice–Boltzmann method to simulate the flow conditions within perfused cell-seeded cylindrical scaffolds. Microcomputed tomography imaging was used to define the scaffold micro-architecture for the simulations, which produced a 3-D fluid velocity field throughout the scaffold porosity. Sucosky et al. (2004) used particle image velocity to determine fluid mechanics of a spinner-flask bioreactor. Coletti et al. (2006) developed a comprehensive mathematical model of convection and diffusion in a perfusion bioreactor, combined with cell growth kinetics. Time-dependent porosity and permeability changes due to the cell density were included in their model. The fluid dynamics of the medium flow inside the bioreactor was described through the Navier–Stokes equations for incompressible fluids while convection through the scaffold was modeled using Brinkman's extension of Darcy's law for porous media. The scaffold porosity $\varepsilon(x_i, t)$, which decreases from its initial value $\varepsilon_0(x_i, 0)$ as the cell density increases, was expressed as follows:

$$\varepsilon(x_i, t) = \varepsilon(x_i, 0) - V_{cell}\rho_{cell}(x_i, t) \tag{41}$$

Where V_{cell} is the single cell volume. Tortuosity was modeled as a function of porosity ε as (Perry and Green (1997):

$$\tau = \left(\frac{2 - \varepsilon}{\varepsilon} \right)^2 \tag{42}$$

The functional form of Koponen et al. (1996) was used for permeability K:

$$K = \frac{\varepsilon^3}{q\tau^2 s^2} \tag{43}$$

Where s is the pore surface area per unit volume of porous material and q is a structural scaffold parameter.

References

Aenis M, Stancampiano AP, Wakhloo AK, and Lieber BB (1997) Modeling of flow in a straight stented and nonstented sidewall aneurysm model. ASME J. Biomech. Eng. 119: 206–212.

AlAmiri A (2000) Analysis of momentum and energy transfer in a lid-driven cavity filled with a porous medium. Int. J. Heat Mass Transfer. 43: 3513–3527.

AlAmiri A (2002) Natural convection in porous enclosures: The application of the two-energy equation model. Num. Heat Transfer: Part A. 41(8): 817–834.

Alazmi B and Vafai K (2002) Constant wall heat flux boundary conditions in porous media under local thermal non-equilibrium conditions. Int. J. Heat Mass Transfer 45: 3071–3087.

Amiri A and Vafai K (1994) Analysis of dispersion effects and nonthermal equilibrium, non-Darcian, variable porosity incompressible-flow through porous media. Int. J. Heat Mass Transfer 37: 939–954.

Amiri A and Vafai K (1998) Transient analysis of incompressible flow through a packed bed. Int. J. Heat Mass Transfer 41: 4259–4279.

Arkin H, Xu LX, and Holmes KR (1994) Recent developments in modeling heat transfer in blood perfused tissues. IEEE Trans. Biomed. Eng. 41: 97–107.

Baish JW (1994) Formulation of a statistical-model of heat transfer in perfused tissue. JASME J. Biomech. Eng. 116: 521–527.

Bancroft GN, Sikavitsast VI, Dolder J van den, Sheffield TL, Ambrose CG, Jansen JA, and Mikos AG (2002) Fluid flow increases mineralized matrix deposition in 3D perfusion culture of marrow stromal osteoblasts in a dose-dependent manner. Proc. Natl. Acad. Sci. USA 99:12600–12605

Bejan A, Dincer I, Lorente S, Miguel A, and Reis A (2004) Porous and complex flow structures in modern technologies. Springer-Verlag, NY.

Canton G, Levy DI, and Lasheras JC (2005) Hemodynamic changes due to stent placement in bifurcating intracranial aneurysms. J. Neusurg. 103: 146–155.

Carrier RL, Papadaki M, Rupnick M, Schoen FJ, Bursac N, Langer R, Freed LE, and Vunjak-Novakovic G (1999) Cardiac tissue engineering: cell seeding, cultivation parameters, and tissue construct characterization. Biotechnol Bioeng 64:580–589

Charny CK (1992) Mathematical models of bioheat transfer. Adv. Heat Transfer 22:19–152.

Charny CK and Levin RL (1988) Heat transfer normal to paired arteries and veins embedded in perfused tissue during hyperthermia. Trans. ASME J. Biomech. Eng. 110: 277–282.

Charny CK and Levin RL (1989) Bioheat transfer in a branching countercurrent network during hyperthermia. ASME J. Biomech. Eng. 111: 263–270.

Chen MM and Holmes KR (1980) Microvascular contributions in tissue heat transfer. Ann. NY Acad. Sci. 335: 137–150.

Coletti F, Macchietto S, and Elvassore N (2006) Mathematical modeling of three-dimensional cell cultures in perfusion bioreactors. Ind. Eng. Chem. Res. 45: 8158–8169.

Dewhirst MW and Samulski TV (1988) Hyperthermia in the treatment for cancer. Upjohn, Kalamazoo, MI.

Field SB and Hand JW (1990) An introduction to the practical aspects of hyperthermia. Taylor & Francis, NewYork.

Gobin YP, Counord JL, Flaud P, and Duffaux J (1994) In vitro study of hemodynamics in a giant saccular aneurysm model: Influence of flow dynamics in the parent vessel and effects of coil embolization. Neuroradiology 36: 530–536.

Groden C, Laudan J, Gatchell S, and Zeumer H (2001) Three-dimensional pulsatile flow simulation before and after endovascular coil embolization of a terminal cerebral aneurysm. J. Cerebr. Blood Flow Met. 21:1464–1471.

Hademenos GJ (1995) The physics of cerebral aneurysms. Phys. Today 48: 25–30.

Ingham DB and Pop I (eds.) (2002) Transport phenomena in porous media, vol. II. Pergamon, Oxford.

Ingham DB and I Pop (eds.) (2005) Transport phenomena in porous media, vol. III. Elsevier, Oxford.

Ingham DB, Bejan A, Mamut E, and Pop I (eds.) (2004) Emerging technologies and techniques in porous media. Kluwer, Dordrecht.

Khanafer K and Vafai K (2001) Isothermal surface production and regulation for high heat flux applications utilizing porous inserts. Int. J. Heat Mass Transfer 44: 2933–2947.

Khanafer K, Vafai K, and Kangarlu A (2003a) Computational modeling of cerebral diffusion-application to stroke imaging. Magn. Reson. Imaging 21:651–661.

Khanafer K, Vafai K, and Kangarlu A (2003b) Water diffusion in biomedical systems as related to magnetic resonance imaging. Magn. Reson. Imaging 21: 17–31.

Khanafer K, Sclicht M, Bull JL, and Berguer R (2006) The role of porous media in finite-element modeling of coil compaction in the treatment of cerebral aneurysms, Proceedings of BIO2006, ASME Summer Bioengineering Conference, Amelia Island Plantation, Florida.

Khanafer KM, Bull JL, Pop I, and Berguer R (2007) Influence of pulsatile blood flow and heating scheme on the temperature distribution during hyperthermia treatment. Int. J. Heat Mass Transfer 50: 4883–4890.

Khashan S, AlAmiri A, Pop I (2005) Assessment of the local thermal non-equilibrium condition in developing forced convection flows through fluid-saturated porous tubes, Appl. Thermal Eng. 25: 1429–1445.

Khashan S, AlAmiri A, Pop I (2006) Numerical simulation of natural convection heat transfer in a porous cavity heated from below using a non-Darcian and thermal non-equilibrium model. Int. J. Heat Mass Transfer 49: 1039–1049.

Klinger HG (1974) Heat transfer in perfused tissue-I: General theory. Bull. Math. Biol. 36: 403–415.

Knuckey N, Haas R, Jenkins R, and Epstein M (1992) Thrombosis of difficult aneurysms by the endovascular placement of platinum-dacron microcoils. J. Neurosurg. 77: 43–50.

Koponen A, Kataja M, and Timonen Jv (1996) Tortuous flow in porous media. Phys. ReV. E: Stat. Phys., Plasmas, Fluids, Relat. Interdiscip. Top 54: 406.

Kwon OK, Kim SH, Oh CW, Han MH, Kang HS, Kwon BJ, Kim JH, and Han DH (2006) Embolization of wide-necked aneurysms with using three or more microcatheters. Acta Neurochir (Wien) 148: 1139–1145.

Lanza R, Langer R, Vacanti JP (2000) Principles of tissue engineering, 2nd ed. Academic Press, New York.

Lanzino G, Wakhloo AK, Fessler RD, Mericle RA, Guterman LR, and Hopkins LN (1998) Intravascular stents for intracranial internal carotid and vertebral artery aneurysms: preliminary clinical experience. Neurosurg. Focus 5(4): E3.

Lavik E and Langer R (2004) Tissue engineering: current state and perspectives. Appl. Microbiol. Biotechnol. 65: 1–8.

Lee DY and Vafai K (1999) Analytical characterization and conceptual assessment of solid and fluid temperature differentials in porous media. Int. J. Mass Transfer 42: 423–435.

Lieber RB, Livescu V, Hopkins LN, and Wakhiloo AK (2002) Particle image velocimetry assessment of stent design influence on intra-aneurysmal flow. Ann. Biomed. Eng. 30: 768–777.

Liou TM, Liou SM, and Chu KL (2004) Intra-aneurysmal flow with helix and mesh stent placement across side-wall aneurysm pore of a straight parent vessel. ASME J. Biomech. Eng. 126: 36–43.

Marafie A and Vafai K (2001) Analysis of non-darcian effects on temperature differentials in porous media. Int. J. Heat Mass Transfer 44: 4401–4411.

Marks MP, Dake MD, Steinberg GK, Norbash AM, and Lane B (1994) Stent placement for arterial and venous cerebrovascular disease: Preliminary clinical experience. Radiology 191: 441–446.

Masood SH, Singh JP, and Morsi Y (2005) The design and manufacturing of porous scaffolds for tissue engineering using rapid prototyping. Int. J. Adv. Manuf. Tech. 27: 415–420.
Nakayama A (1995) PC-Aided numerical heat transfer and convective flow. CRC Press, Tokyo.
Nield DA and Bejan A (2006) Convection in porous media, 3rd ed. Springer, New York.
Ohta M, Wetzel SG, Dantan P, Bachelet C, Lovblad KO, Yilmaz H, Flaud P, and Rufenacht DA (2005) Rheological changes after stenting of a cerebral aneurysms: A finite element modeling approach. Cardiovasc. Inter. Rad. 28: 768–772.
Oleson JR, Sim DA, and Manning MR (1984) Analysis of prognostic variables in hyperthermia treatment of 161 patients. Int. J. Radiat. Oncol. Biol. Phys. 10: 2231–2239.
Overgaard J, Gonzales DG, Hulshof MC, Arcangeli G, Dahl O, Mella O, and Bentzen SM (1996) Hyperthermia as an adjuvant to radiation therapy of recurrent or metastatic melanoma: A multicenter randomized trial by the European society for hyperthermic oncology. Int. J. Hyperth. 12: 3–20.
Pennes HH (1948) Analysis of tissue and arterial blood temperature in the resting human forearm. J. Appl. Physiol. 1: 93–122.
Perry RH and Green DW (1997) Perry's chemical engineer handbook, 7th ed. McGraw-Hill, New York.
Pop I and Ingham DB (2001) Convective heat transfer: Mathematical and computational modeling of viscous fluids and porous media. Pergamon, Oxford.
Port F (2002) OPTN/SRTS annual report. Scientific Registry of Transplant Recipients and Organ Procurement Transplantation Network, Washington, D.C.
Porter B, Zauel R, Stockman H, Robert G, and Fyhrie D (2005) 3-D computational modelling of media flow through scaffolds in a perfusion bioreactor. J. Biomech. 38: 543–549.
Rhee K, Han MH, and Cha SH (2002) Changes of flow characteristics by stenting in aneurysm models: Influence of aneurysm geometry and stent porosity. Ann. Biomed. Eng. 30: 894–904.
Roemer RB and Cetas TC (1984) Applications of bioheat transfer simulations in hyperthermia. Cancer Res. 44: 4788–4798.
Sikavitsas VI, Bancroft GN, and Mikos AG (2002) Formation of three dimensional cell/polymer constructs for bone tissue engineering in a spinner flask and a rotating wall vessel bioreactor. J. Biomed. Mater. Res. 62:136–148
Srinivasan V, Vafai K, and Christensen RN (1994) Analysis of heat transfer and fluid flow through a spirally fluted tube using a porous substrate approach. ASME J. Heat Transfer 116: 543–551.
Stuhne GR and Steinman DA (2004) Finite-element modeling of the hemodynamics of stented aneurysm. ASME J. Biomech. Eng. 126: 382–212.
Sucosky P, Osorio DF, Brown JB, Neitzel G (2004) Fluid mechanics of a spinner- flask bioreactor. Biotechnol. Bioeng 85: 34–46.
Szikora I, Guterman LR, Wells KM, et al. (1994) Combined use of stents and coils to treat experimental wide-necked carotid aneurysms: Preliminary results. AJNR 15:1091–1102.
Turjman F, Massoud TF, Ji C, et al. (1994) Combined stent implantation and endosaccular coil placement for treatment of experimental wide-necked aneurysms: A feasibility study in swine. AJNR 12:1087–1090.
Vafai K (1984) Convective flow and heat transfer in variable-porosity media. J. Fluid Mech. 147: 233–259.
Vafai K (1986) Analysis of the channeling effect in variable porosity media. ASME J. Energy Resour. Technol. 108: 131–139.
Vafai K (ed.) (2000) Handbook of porous media. Marcel Dekker, New York.
Vafai K (ed.) (2005) Handbook of porous media, 2nd ed. Taylor & Francis, New York.
Vafai K and Amiri A (1998) Non-Darcian effects in confined forced convective flows, Transport Phenomena in Porous Media. D.B. Ingham and I. Pop (Eds.), 313–329, Pergamon, UK.
Vafai K and Tien CL (1980) Boundary and inertia effects on flow and heat transfer in porous media. Int. J. Heat Mass Transfer 24:195–203.
Vafai K and Tien C L (1981) Boundary and inertia effects on convective mass transfer in porous media. Int. J. Heat Mass Transfer 25:1183–1190.

Wakhloo AK, Schellhammer F, de Vries J, et al. (1994a): Self-expanding and balloon-expandable stents in the treatment of carotid aneurysms: An experimental study in a canine model. AJNR 15: 493–502.

Wakhloo AK, Schellhammer F, Vries JD, Haberstroh J, and Schumacher M (1994b) Self-Expanding and balloon-expandable stents in the treatment of carotid aneurysms: An experimental study in a canine model. AJNR: AM J. Neurosurg. 15: 493–502.

Wakhloo AK, Tio FO, Lieber BB, et al. (1995) Self-expanding nitinol stents in canine vertebral arteries: Hemodynamics and tissue response. AJNR 16:1043–1051.

Wakhloo AK, Lanzino G, Lieber BB, et al. (1998) Stents for intracranial aneurysms: the beginning of a new endovascular era? Neurosurgery 43: 377–379.

Weinbaum S and Jiji LM (1979) A two phase theory for the influence of circulation on the heat transfer in surface tissue. In 1979 Advances in Bioengineering (M.K. Wells, ed.): 179–182, NY.

Weinbaum S, Jiji LM, and Lemons DE (1984a) Theory and experiment for the effect of vascular microstructure on surface tissue heat transfer. Part I. Anatomical foundation and model conceptualization. ASME J. Biomech. Eng.106: 321–330.

Weinbaum S, Jiji LM, and Lemons DE (1984b) Theory and experiment for the effect of vascular microstructure on surface tissue heat transfer. Part II. Model formulation and solution. ASME J. Biomech. Eng. 106: 331–341.

Weinbaum S and Jiji LM (1985) A new simplified equation for the effect of blood flow on local average tissue temperature. ASME J. Biomech. Eng. 107: 131–139.

Wissler EH (1987) Comments on the new bioheat equation proposed by Weinbaum and Jiji. ASME J. Biomech. Eng. 109: 226–232.

Wulff W(1974) The energy conservation equation for living tissues. IEEE Trans. Biomed. Eng. BME 21: 494–495.

Xuan YM and Roetzel W (1997) Bioheat equation of the human thermal system. Chem. Eng. Technol. 20: 268–276.

Xuan YM and Roetzel W (1998) Transfer response of the human limb to an external stimulus. Int. J. Heat Mass Transfer 41: 229–239.